HHS Public Access

Author manuscript

Semin Immunopathol. Author manuscript; available in PMC 2015 April 28.

Published in final edited form as:

Semin Immunopathol. 2010 September ; 32(3): 297–304. doi:10.1007/s00281-010-0209-9.

Two-photon microscopy in pulmonary research

Ruben G. Nava,
Department of Surgery, Washington University in St. Louis, St. Louis, MO, USA

Wenjun Li,
Department of Surgery, Washington University in St. Louis, St. Louis, MO, USA

Andrew E. Gelman,
Department of Surgery, Washington University in St. Louis, St. Louis, MO, USA

Department of Pathology and Immunology, Washington University in St. Louis, Campus Box 8234, 660 South Euclid Avenue, St. Louis, MO 63110-1013, USA

Alexander S. Krupnick,
Department of Surgery, Washington University in St. Louis, St. Louis, MO, USA

Mark J. Miller, and
Department of Pathology and Immunology, Washington University in St. Louis, Campus Box 8234, 660 South Euclid Avenue, St. Louis, MO 63110-1013, USA

Daniel Kreisel
Department of Surgery, Washington University in St. Louis, St. Louis, MO, USA

Department of Pathology and Immunology, Washington University in St. Louis, Campus Box 8234, 660 South Euclid Avenue, St. Louis, MO 63110-1013, USA

Daniel Kreisel: kreiseld@wudosis.wustl.edu

Abstract

As the lung is constantly exposed to both innocuous and potentially noxious antigens, a thorough understanding of both innate and adaptive immune responses in this organ is of the essence. Imaging modalities such as magnetic resonance imaging, positron emission tomography, and confocal microscopy have expanded our knowledge about various molecular processes and cellular responses in the lung. Two-photon microscopy has evolved into a powerful tool to observe cellular interactions in real time and has markedly expanded our understanding of the immune system. Recently, two-photon microscopy has also been utilized to image the murine lung. As immune responses in the lung differ from those in other non-lymphoid tissues, this technique holds great promise to advance our knowledge of the biology that underlies a wide spectrum of pulmonary diseases.

Correspondence to: Daniel Kreisel, kreiseld@wudosis.wustl.edu.

Keywords

Lung; Immune responses; Imaging; Two-photon microscopy

Pulmonary immune responses

The large epithelial surface area of the lung is an important interface between the body and the environment. Largely due to constant exposure to many infectious and noxious agents as well as antigens, lungs are a key site for multiple human diseases that have a great impact on public health. Bacterial and viral respiratory infections are the most common infectious illnesses in humans and are associated with significant morbidity and mortality. Worldwide, lung infections are the third most common cause of death and the leading cause of mortality among children [34]. Moreover, allergic asthma affects millions of patients worldwide, and its prevalence is rising. While the pathogenesis of asthma is highly complex, it is generally accepted that T_h2 cytokines play an important role [21]. Primary lung cancers as well as metastatic disease of the lung are the leading causes of malignancy-related morbidity and death in the Western world. Both experimental and clinical studies have clearly indicated that the immune system regulates the growth of tumors [23]. Although inhalational administration of antigens can lead to immune tolerance, lung allografts are particularly immunogenic and are associated with markedly high rates of rejection [1, 15]. Immune-mediated processes also play an important role in other diseases affecting the lungs such as emphysema and berylliosis [38, 41]. Thus, the lung is an organ of critical importance to immunologists. A better understanding of the pathogenesis of immune-mediated processes in the lung may ultimately lead to the design of host-protective strategies to combat infections and tumors as well as allow for the design of therapeutic approaches to ameliorate deleterious immune responses in asthma and lung transplantation.

Lung imaging modalities

Imaging studies have been instrumental in elucidating pathogenetic mechanisms in a wide variety of rodent models of human disease [19]. To this end, several techniques have been utilized to visualize biological processes in murine lungs. Traditionally, such techniques have been generally divided into those that are able to provide descriptions of anatomical structure and those that allow for functional investigations. Recent advances such as high-resolution instruments as well as the development of specific molecular probes have significantly expanded the armamentarium available to biomedical investigators to image, monitor, and quantify molecular and cellular pulmonary processes. Modalities that have been used increasingly for imaging of murine lungs are magnetic resonance imaging (MRI), positron emission tomography (PET), and fluorescence microscopy.

MRI is a non-ionizing imaging technique that uses powerful magnetic and radio frequency fields to systematically alter the alignment of hydrogen nuclei (magnetic moments) in tissues. When hydrogen nuclei return to their normal state, photons are released and detected by the scanner to construct an image. In the mouse, in vivo MRI of the lung has been somewhat challenging due to the constant motion as well as relatively low tissue content and abundant air–tissue interfaces resulting in poor signals. The importance of MRI in

pulmonary research stems in large part from its ability to visualize 3D morphology, thereby providing anatomical detail. Furthermore, it allows investigators to examine temporal changes in a noninvasive fashion and has therefore been used for the study of several pulmonary disease processes. Using breathable gases that provide strong MR signals such as hyperpolarized ^{3}He, this imaging modality can be used for the study of asthma. To this end, Driehuys et al. [12] recently demonstrated airway narrowing and loss of ventilation in ovalbumin-sensitized metacholine-challenged mice. Notably, airways up to their fifth generation could be visualized in this study. MRI has been frequently used to assess pulmonary tumor growth, and our group has recently utilized MRI to assess intact ventilation in long-term surviving syngeneic mouse lung transplants [6, 35]. Notably, a recent study reported the ability to track adoptively transferred mesenchymal stem cells, labeled ex vivo with magnetic iron nanoparticles, within metastatic pulmonary tumors by MRI [28].

In PET, typically an analogue of glucose containing the radioactive isotope fluorine-18 is injected into the subject. As the radioisotope undergoes positron emission decay, it emits a positron, which collides with an electron producing gamma rays. The gamma rays are detected by a scintillator, creating visible light, which is detected by photomultiplier tubes or avalanche photodiodes. As the tracer decays, images of tracer concentration over time are reconstructed in 3D by computer. The development of micro-PET scanners that have spatial resolutions of 2 mm or less has enabled investigators to utilize PET imaging in mice. This molecular imaging technique has been used to monitor gene expression in mouse lungs. PET imaging of murine lungs relies on the intravenous or, more commonly, intratracheal delivery of a viral or non-viral vector that carries a reporter transgene [11]. Importantly, the protein product of the reporter transgene must have the capacity to trap a reporter probe in order to study transgene expression. Advantages of PET imaging include its high sensitivity and its ability to detect tracer located deep within the lung tissue. The value of PET imaging to monitor pulmonary gene expression has been recently illustrated in a model of orthotopic vascularized single-lung transplantation in the rat [10]. Lungs of donor animals were transfected via endotracheal administration of a replication-deficient adenoviral vector containing a fusion gene of a mutant variant of the murine herpes simplex virus type I thymidine kinase as the reporter gene and green fluorescent protein driven by the constitutive cytomegalovirus promoter 24 h prior to organ harvest. The product of this reporter gene was able to convert the radioactive reporter probe 9-(4-[^{18}F]fluoro-3-hydroxymethylbutyl)guanine, which was injected into recipient rats 1 h prior to PET imaging, to a metabolite that was trapped within transfected pulmonary cells. PET imaging was able to detect transgene expression in transfected lungs even in the presence of severe injury related to either acute rejection or ischemia–reperfusion following prolonged cold storage. The great potential of applying donor-directed gene therapy in lung transplantation has been further substantiated by a recent report that ex vivo endobronchial transfection of donor lungs with an adenovirus containing IL-10 leads to a marked improvement in their function [9]. Undoubtedly, PET imaging will play an important role in future studies to assess and monitor pulmonary transgene expression in lung transplantation and other pulmonary disease processes. In addition, combining PET imaging with computed

tomography offers the advantage of assessing gene expression in the context of detailed structural delineation [22].

Intravital pulmonary microscopy can be conducted in ventilated lungs of live animals [24]. To address the obvious technical hurdle of cardiorespiratory movement in live animals, Wagner [44] devised a thoracic window to stabilize portions of canine lungs during microscopic evaluation of the subpleural pulmonary microcirculation. Similar techniques have subsequently enabled investigators to use intravital microscopy to visualize the pulmonary microcirculation and examine cellular trafficking of ex vivo or in vivo fluorescently labeled cells within the subpleural vessels of ventilated rabbit or rat lungs [25, 29]. More recently, Tabuchi et al. [42] applied the thoracic window technique to mice where a circular defect was created in the right chest wall by excising portions of the third, fourth, and fifth ribs, which was subsequently covered with a transparent membrane. Intravenous fluorescein isothiocyanate (FITC)–dextran was used to visualize subpleural pulmonary vessels and their response to hypoxic conditions. Furthermore, ex vivo labeling of platelets with fluorochromes allowed the investigators to detect their sequestration within the vasculature. Importantly, this preparation did not result in hemodynamic alterations or structural changes of the imaged lung over a 2-h period. Another approach to image lungs with intravital microscopy is the use of isolated, perfused organ preparations, which has been reported in several species including mice [4, 32]. The use of fluorescent probes has facilitated the visualization of cytosolic and nuclear processes within pulmonary cells in real time. For example, such studies have yielded mechanistic insight into surfactant secretion by alveolar type II epithelial cells in response to stretch in isolated perfused rat lungs [2]. An elegant application of intravital lung microscopy has been recently reported by Cortez-Retamozo et al. [8] where the injection of enzyme-targeted (i.e., matrix metalloproteinase) optical sensors allowed the visualization of eosinophils in inflamed lungs. While confocal microscopy has provided significant insight into lung biology, this methodology has some limitations. Images acquired deep inside biological tissues with confocal microscopy are often degraded due to light scattering. Therefore, the imaging capability of confocal microscopy is restricted to relatively superficial areas of the lung. However, many innate and adaptive immune responses such as antigen recognition occur deep within secondary lymphoid organs. Imaging lungs at depths of >100 μm would make it possible to see immune responses in the air spaces and study leukocyte trafficking in deeper vessels of the pulmonary microcirculation.

Two-photon microscopy of the lung

By enabling investigators to observe the dynamic interactions of different cell populations in real time, two-photon (2P) microscopy has significantly broadened our understanding of cellular immunity in a variety of tissues. Importantly, 2P microscopy has allowed for the in vivo confirmation of observations and findings that had been previously described in vitro [5]. While in vitro experiments have led to significant advances in pulmonary research, generally they provide only a stationary picture of a dynamic process, and isolating and manipulating cells ex vivo can affect their function. The value of in situ imaging of immune responses in the lung is further illustrated by the observations that the anatomical location of

antigen-presenting cells within different compartments of the lung can have functional consequences [43].

The concept of 2P excitation was first described by the Physics Nobelist Maria Göppert-Mayer in 1931 [17]. With 2P excitation, energy from two photons are absorbed by the fluorophore nearly simultaneously, with each photon providing half of the energy necessary to promote an electron to an excited state. As the excited electron returns to the ground state, the remaining energy after non-radiative loss is released as a photon, in a process identical to single-photon-induced fluorescence. Largely due to significant developments in lasers and computer-controlled systems, the use of 2P microscopy in biomedical research has steadily increased over the last decade [13, 20]. This imaging approach typically requires the use of fluorescent labels in order to observe cells of interest. This can be accomplished simply by the adoptive transfer of cells that have been labeled ex vivo with fluorescent dyes [45]. Examples of commonly used fluorescent dyes include 5-(and 6)-carboxyfluorescein diacetate succinimidyl ester (CFSE), 5-(and-6)-(((4-chloromethyl)benzoyl)amino)tetramethylrhodamine (CMTMR), and 7-amino-4-chloromethylcoumarin (CMAC). Alternatively, cells that express various fluorescent proteins such as green fluorescent protein (GFP) or yellow fluorescent protein (YFP) can be imaged with 2P microscopy. This can be accomplished by generating transgenic mice that express these proteins under the control of a specific promoter. An example that we and others have used is the CD11c-EYFP mouse that expresses enhanced YFP under a CD11c promoter and allows for the visualization of dendritic cells or macrophages [15, 27]. This mouse has been instrumental in 2P microscopic investigations examining interactions between antigen-presenting cells and T lymphocytes. As outlined above, FITC–dextran has been used to label subpleural capillary vessels [42]. More recently, we and others have used quantum dots to label blood vessels [16]. 2P microscopy can also produce intrinsic signals, such as the autofluorescence given off by alveolar macrophages or the second harmonic generation (SHG) signal produced as the laser interacts with birefringent materials, for example collagen, which yields a signal of approximately half the laser excitation wavelength. The main advantages of 2P microscopy compared to single-photon techniques such as confocal microscopy are that excitation is restricted to a small volume in the sample, thereby inducing less sample photobleaching and photodamage, and near-infrared laser light scatters less in biological materials, permitting deeper tissue imaging [20]. The value of 2P microscopy is that single-cell dynamics can be studied in the context of their native 3D tissue environments.

2P microscopy has been used to image both explanted tissues as well as organs in live anesthetized mice. Both experimental approaches have advantages and disadvantages. While imaging of explants allows for comparably easier tissue positioning and enables visualization of deeper areas after slicing the specimen, it involves surgical trauma related to the removal of the tissue from its physiological environment. Moreover, the imaged tissue lacks blood flow, and maintenance of the tissue relies on its immersion in oxygenated and temperature-controlled media. In contrast, in vivo imaging reflects physiological conditions in the animal. However, there are issues related to anesthesia of the animal and restraint of the tissue that can present significant technical challenges and possibly introduce untoward artifacts.

Compared to other tissues such as lymph nodes, where 2P microscopy has been used extensively over the last few years, only a few studies have applied this technology to examine immune and non-immune processes within the lung. In 2006, St. Croix et al. [40] compared 2P imaging with single-photon confocal microscopy of lung tissue ex vivo. They applied these imaging modalities to two distinct pulmonary processes, namely, hypoxic pulmonary vasoconstriction and interactions of adoptively transferred natural killer cells with lung tumors. In order to study the interactions of natural killer cells with pulmonary tumors, animals were injected with tumors that were transduced with GFP. Following the establishment of these tumors within the lung, the authors adoptively transferred natural killer cells that had been labeled with rhodamine. Using single-photon confocal microscopy to visualize events within these lung explants, static high-resolution images of natural killer cells interacting with tumors could be generated up to depths of approximately 200 μm. Compared to single-photon confocal microscopy, multi-photon imaging offered the important advantage of improved tissue penetration with the ability to image cellular interactions at markedly deeper levels of approximately 500 μm. In addition, injection of fluorochrome-labeled latex beads enabled these investigators to visualize the tumor vasculature, thereby allowing them to make more definitive statements about the precise location and trafficking of natural killer cells within the tumors. Hypoxic pulmonary vasoconstriction, a lung-specific autoregulatory mechanism originally described by Euler and Liljestrand, is critical in the regulation of pulmonary arterial blood flow [39]. Pulmonary arterial blood flow is redirected from alveoli with relative hypoxemia to alveoli that have higher oxygen tension, thereby preventing intrapulmonary shunting and reducing ventilation–perfusion mismatches. The authors imaged perfused lungs derived from Tie2-GFP mice which express GFP under an endothelial-specific promoter. While, due to its comparably low tissue penetration, confocal microscopy allowed the investigators to study changes of pulmonary vessel sizes in response to hypoxic conditions only in the subpleural capillary network, multiphoton imaging allowed for the examination of vessels deeper within the lung tissue.

A topic that has been debated for several decades is the site of the initiation of an adaptive immune response following transplantation of allogeneic grafts. Recent seminal studies in this field have established that secondary lymphoid organs such as spleen and lymph nodes are critical in order to trigger acute rejection of hearts or skin [26]. These observations indicated that activation of recipient T cells depends on their encounter of alloantigen-presenting cells within secondary lymphoid organs. In contrast, our group has recently described that lungs can be rejected in the absence of secondary lymphoid organs [15]. Importantly, we utilized 2P microscopy to visualize the initiation of an immune response to a lung allograft, which, to our knowledge, was the first use of this imaging modality in transplantation biology [15]. We transplanted CD11c-EYFP lungs into allogeneic hosts and imaged the graft explants with 2P microscopy on the following day. Compared to T cells in syngeneic grafts or random Monte Carlo simulations, we observed that T cells within lung allografts had significantly more neighbors. Such T cell clustering has been described as a sensitive readout of their priming and temporally correlated with their expression of CD69, an early T lymphocyte activation marker. Furthermore, we observed that many T cells in lung allografts clustered around donor-derived $CD11c^+$ cells with a dendritic morphology.

Thus, 2P imaging provided compelling evidence that a lung graft provides a suitable environment for the activation of alloreactive T cells, setting lung transplants apart from other solid organ grafts. These observations also provide a potential explanation for the high immunogenicity of lung grafts as well as the previously documented rapid onset of lung rejection in humans [30]. Furthermore, using CD11c-EYFP mice as lung recipients, we have recently demonstrated by 2P microscopy that T lymphocytes also interact with host $CD11c^+$ antigen-presenting cells within pulmonary allografts. Interestingly, graft-infiltrating recipient $CD11c^+$ antigen-presenting cells can express MHC molecules of both donor and host origin and can therefore contribute to the activation of direct and indirect allorecognition pathways [14].

These findings extended previous observations that adaptive immune responses following respiratory viral infections can be generated within the lung [33]. However, unlike the case in lung allografts where we could not detect the expression of markers that are characteristic of organized bronchus-associated lymphoid tissue (BALT), these viral studies established inducible BALT as an important site where adaptive immune responses could be initiated within the murine lung. Unlike other species, mice do not express BALT constitutively, but it can be induced under inflammatory conditions. Similar to secondary lymphoid organs, such tissue is well organized with B cell follicles, which are surrounded by T cell zones. The expression of homeostatic chemokines such as CCL21 and CXCL13 is important for the structural organization of BALT [37]. Furthermore, trafficking of T cells through BALT is facilitated by interactions of their homing receptors with peripheral lymph node addressin, a molecule expressed on high endothelial venules. Halle et al. [18] recently employed ex vivo 2P microscopy to gain further mechanistic insight into the role of inducible BALT as a priming site for naïve T cells. Intranasal infection of mice with the replication-deficient modified vaccinia virus Ankara (MVA) resulted in the induction of BALT. The authors demonstrated that $CD11c^+$ cells play an important role in both the organization and the maintenance of inducible BALT. For the purpose of 2P imaging, 1- to 2-mm-thick horizontal lung slices were placed in a chamber that was perfused with oxygenated medium allowing for dynamic investigations of cellular interactions, similar to techniques previously reported for the ex vivo imaging of secondary lymphoid organs [31]. The investigators observed that intratracheally administered antigen-loaded GFP-expressing dendritic cells interacted with antigen-specific fluorochrome-labeled adoptively transferred antigen-specific $CD8^+$ T cells within BALT that had been previously induced through intranasal infection with MVA. Compared to polyclonal $CD8^+$ T cells, antigen-specific $CD8^+$ T lymphocytes formed stable contacts with dendritic cells and were significantly less motile. Interestingly, dynamic images revealed some movement of the dendritic cell dendrites, which was interpreted as probing activity during antigen presentation. Overall, interactions between antigen-specific T lymphocytes and antigen-presenting cells within induced BALT resembled those observed in secondary lymphoid organs. Notably, in addition to imaging of T lymphocytes and dendritic cells, 2P microscopy was able to visualize structural components of the lung in this study such as bronchi and vessels based on their autofluorescence and the SHG signal produced by collagen fibers.

In this context, Pena et al. [36] took advantage of the ability to visualize unstained extracellular matrix by 2P microscopy and thereby delineate a 3D structure to examine and

quantify fibrotic processes within the lung. In a mouse model, pulmonary fibrosis was induced by intratracheal administration of bleomycin. Lung tissue was imaged with 2P laser scanning microscopy at 860-nm excitation. The SHG signal, in combination with 2P-excited fluorescence, was used to quantify the fibrosis. At these settings, the SHG signal and 2P-excited fluorescence signals are emitted at 430 nm and wavelengths longer than 430 nm, respectively. Detection of fibrillar collagen through SHG signals was validated through staining of analogous histological sections with picrosirius, a method that had been established several decades ago to selectively stain collagen [7]. 2P-excited fluorescence signals detected elastin, which was validated by staining histological sections with orcein. 2P-excited fluorescence signals were generated by several structures in the lung, including arterioles, bronchioles, and alveolar macrophages. Bleomycin treatment resulted in an early and transient increase in 2P-excited fluorescence density from days 3 to 7, which was the result of an increased accumulation of inflammatory cells such as alveolar macrophages. The SHG signal demonstrated a marked and heterogeneous accumulation of collagen within the lung, both subpleurally as well as in the alveolar interstitium, which was first documented on day 3 and progressed to marked fibrosis by day 14. Interestingly, the authors extended these observations to human tissue as well, where 2P imaging was used to visualize the fibrotic remodeling in lung biopsies from idiopathic pulmonary fibrosis patients. Based on these observations, these investigators suggested that 2Pmicroscopy could be a valuable approach to assess both extent and distribution of fibrotic processes in a wide variety of organs.

In a recent study, Bakocevic et al. [3] labeled pulmonary dendritic cells through intratracheal administration of ovalbumin-loaded fluorescent latex beads and used 2P microscopy to examine their interactions with ovalbumin-specific DO11.10 $CD4^+$ T lymphocytes within explanted bronchial lymph nodes. Ovalbumin-loaded fluorescent latex beads were administered with or without LPS to mirror inflammatory and non-inflammatory conditions, respectively. Irrespective of addition of LPS, antigen-specific $CD4^+$ T cells displayed similar patterns of motility with comparable velocities within the bronchial lymph nodes. The authors also analyzed arrest coefficients for the $CD4^+$ T cells, which is an indicator of the formation of stable contacts between antigen-presenting cells and T lymphocytes. Notably, they observed increased arrest coefficients for antigen-specific $CD4^+$ T lymphocytes at early time points under inflammatory conditions. Moreover, when LPS was administered with the ovalbumin-loaded fluorescent latex beads, dendritic cells formed longer lasting, more stable clusters with $CD4^+$ T lymphocytes.

An experimental setup for imaging lung explants is outlined below to demonstrate the utility of 2P microscopy. Here, we purified C57BL/6 T cells with magnetic beads and labeled these cells with fluorescent dyes (CMTMR or CMAC) as previously described [45]. After labeling, equal numbers of CMTMR- and CMAC-labeled T cells were injected into a transgenic CD11c-EYFP mouse, and 24 h later, their lungs were imaged. In order to label blood vessels, we injected quantum dots 10 min prior to killing the mice for imaging. The lungs of the mouse were extracted and placed in a Petri dish with DMEM medium. The imaging chamber was placed on the microscope stage and filled with warmed medium through the inlet line. The peristaltic pump was adjusted to provide a constant flow through the in-line heater and into the chamber. A vacuum line was attached to aspirate excess of

medium from the chamber. The chamber heater was connected and adjusted to 37°C (Fig. 1a, b). Lung tissue was glued to a plastic cover slip and submerged inside the imaging chamber (Fig. 1c). The one Ti:Sapphire laser was tuned to 890 nm and a second laser tuned to 820 nm. The dichroic filters used in this particular experiment to separate the florescence emission signals were 458 and 570 nm, which provide a good separation of the CMAC- (cyan), YFP- (yellow-green), and CMTMR- (orange) labeled cells in our hands (Fig. 1d). Figure 2 depicts two different areas of the same lung explant. The power of the first laser was maintained at 25–30%, and the power of the second laser was turned up to 80% to image the SHG signal, which appeared a deep blue using these optical settings. Peri-alveolar blood vessels labeled with quantum dots appear red and the CD11c-EYFP cells of the host mouse are seen in yellow-green (Fig. 2a). Several cell types within the lung can express CD11c, including dendritic cells and macrophages, and in this experiment, different $CD11c^{+}$ cells can be distinguished based on morphological characteristics. Alveolar macrophages have a characteristically compact morphology with a nuclear shadow and lack dendrites and can therefore be easily distinguished from dendritic cells (Fig. 2b).

Conclusions

The lung constitutes one of the first lines of defense against antigens, which is in large part due to a large epithelial surface area and its constant exposure to the external environment. Thus, a better understanding of innate and adaptive immune responses in the lung is critical for the development of improved protective strategies. Although at the present time only few studies have utilized 2P microscopy to image the lung, this modality holds great promise to advance pulmonary research. Largely because of challenges related to respiratory and cardiac motion, the use of in vivo 2P intravital microscopy to study single-cell dynamics in the lung has not been reported to date. Our group has recently developed techniques that allow for intravital 2P imaging of mouse lungs, which we expect to be useful for the study of cellular trafficking behavior at steady state as well as in a wide variety of models examining pulmonary disease processes. Nevertheless, although in vivo imaging may arguably represent the most accurate representation of physiological events, the cited studies illustrate that ex vivo 2P imaging of whole lungs or lung sections have already yielded and will continue to provide valuable insight into pulmonary biology.

References

1. Aramaki O, Shirasugi N, Takayama T, Shimazu M, Kitajima M, Ikeda Y, Azuma M, Okumura K, Yagita H, Niimi M. Programmed death-1–programmed death-L1 interaction is essential for induction of regulatory cells by intratracheal delivery of alloantigen. Transplantation. 2004; 77:6–12. [PubMed: 14724428]
2. Ashino Y, Ying X, Dobbs LG, Bhattacharya J. [Ca(2+)](i) oscillations regulate type II cell exocytosis in the pulmonary alveolus. Am J Physiol Lung Cell Mol Physiol. 2000; 279:L5–L13. [PubMed: 10893197]
3. Bakocevic N, Worbs T, Davalos-Misslitz A, Forster R. T cell-dendritic cell interaction dynamics during the induction of respiratory tolerance and immunity. J Immunol. 2010; 184:1317–1327. [PubMed: 20042584]
4. Bernal PJ, Leelavanichkul K, Bauer E, Cao R, Wilson A, Wasserloos KJ, Watkins SC, Pitt BR, St Croix CM. Nitric-oxide-mediated zinc release contributes to hypoxic regulation of pulmonary vascular tone. Circ Res. 2008; 102:1575–1583. [PubMed: 18483408]

5. Cahalan MD, Parker I, Wei SH, Miller MJ. Real-time imaging of lymphocytes in vivo. Curr Opin Immunol. 2003; 15:372–377. [PubMed: 12900266]
6. Carreno BM, Garbow JR, Kolar GR, Jackson EN, Engelbach JA, Becker-Hapak M, Carayannopoulos LN, Piwnica-Worms D, Linette GP. Immunodeficient mouse strains display marked variability in growth of human melanoma lung metastases. Clin Cancer Res. 2009; 15:3277–3286. [PubMed: 19447870]
7. Constantine VS, Mowry RW. Selective staining of human dermal collagen. I. An analysis of standard methods. J Invest Dermatol. 1968; 50:414–418. [PubMed: 4172461]
8. Cortez-Retamozo V, Swirski FK, Waterman P, Yuan H, Figueiredo JL, Newton AP, Upadhyay R, Vinegoni C, Kohler R, Blois J, Smith A, Nahrendorf M, Josephson L, Weissleder R, Pittet MJ. Real-time assessment of inflammation and treatment response in a mouse model of allergic airway inflammation. J Clin Invest. 2008; 118:4058–4066. [PubMed: 19033674]
9. Cypel M, Liu M, Rubacha M, Yeung JC, Hirayama S, Anraku M, Sato M, Medin J, Davidson BL, de Perrot M, Waddell TK, Slutsky AS, Keshavjee S. Functional repair of human donor lungs by IL-10 gene therapy. Sci Transl Med. 2009; 1:4ra9.
10. Dharmarajan S, Hayama M, Kozlowski J, Ishiyama T, Okazaki M, Factor P, Patterson GA, Schuster DP. In vivo molecular imaging characterizes pulmonary gene expression during experimental lung transplantation. Am J Transplant. 2005; 5:1216–1225. [PubMed: 15888025]
11. Dharmarajan S, Schuster DP. Molecular imaging of pulmonary gene expression with positron emission tomography. Proc Am Thorac Soc. 2005; 2(549–552):514–546.
12. Driehuys B, Walker J, Pollaro J, Cofer GP, Mistry N, Schwartz D, Johnson GA. ^{3}He MRI in mouse models of asthma. Magn Reson Med. 2007; 58:893–900. [PubMed: 17969115]
13. Dunn KW, Young PA. Principles of multiphoton microscopy. Nephron Exp Nephrol. 2006; 103:e33–e40. [PubMed: 16543762]
14. Gelman AE, Okazaki M, Sugimoto S, Li W, Kornfeld CG, Lai J, Richardson SB, Kreisel FH, Huang HJ, Tietjens JR, Zinselmeyer BH, Patterson GA, Miller MJ, Krupnick AS, Kreisel D. CCR2 regulates monocyte recruitment as well as CD4 T1 allorecognition after lung transplantation. Am J Transplant. 2010; 10:1189–1199. [PubMed: 20420631]
15. Gelman AE, Li W, Richardson SB, Zinselmeyer BH, Lai J, Okazaki M, Kornfeld CG, Kreisel FH, Sugimoto S, Tietjens JR, Dempster J, Patterson GA, Krupnick AS, Miller MJ, Kreisel D. Cutting edge: acute lung allograft rejection is independent of secondary lymphoid organs. J Immunol. 2009; 182:3969–3973. [PubMed: 19299693]
16. Germain RN, Miller MJ, Dustin ML, Nussenzweig MC. Dynamic imaging of the immune system: progress, pitfalls and promise. Nat Rev Immunol. 2006; 6:497–507. [PubMed: 16799470]
17. Goeppert-Mayer M. Elementary processes with two quantum transitions. Annalen der Physik. 2009; 18:466–479.
18. Halle S, Dujardin HC, Bakocevic N, Fleige H, Danzer H, Willenzon S, Suezer Y, Hammerling G, Garbi N, Sutter G, Worbs T, Forster R. Induced bronchus-associated lymphoid tissue serves as a general priming site for T cells and is maintained by dendritic cells. J Exp Med. 2009; 206:2593–2601. [PubMed: 19917776]
19. Hedlund LW, Johnson GA. Morphology of the small-animal lung using magnetic resonance microscopy. Proc Am Thorac Soc. 2005; 2:481–483. 501–482. [PubMed: 16352752]
20. Helmchen F, Denk W. Deep tissue two-photon microscopy. Nat Methods. 2005; 2:932–940. [PubMed: 16299478]
21. Kitajima M, Iwamura C, Miki-Hosokawa T, Shinoda K, Endo Y, Watanabe Y, Shinnakasu R, Hosokawa H, Hashimoto K, Motohashi S, Koseki H, Ohara O, Yamashita M, Nakayama T. Enhanced Th2 cell differentiation and allergen-induced airway inflammation in Zfp35-deficient mice. J Immunol. 2009; 183:5388–5396. [PubMed: 19783676]
22. Kligerman S, Digumarthy S. Staging of non-small cell lung cancer using integrated PET/CT. AJR. Am J Roentgenol. 2009; 193:1203–1211. [PubMed: 19843732]
23. Koebel CM, Vermi W, Swann JB, Zerafa N, Rodig SJ, Old LJ, Smyth MJ, Schreiber RD. Adaptive immunity maintains occult cancer in an equilibrium state. Nature. 2007; 450:903–907. [PubMed: 18026089]

24. Kuebler WM, Parthasarathi K, Lindert J, Bhattacharya J. Real-time lung microscopy. J Appl Physiol. 2007; 102:1255–1264. [PubMed: 17095639]
25. Kuhnle GE, Leipfinger FH, Goetz AE. Measurement of microhemodynamics in the ventilated rabbit lung by intravital fluorescence microscopy. J Appl Physiol. 1993; 74:1462–1471. [PubMed: 8482691]
26. Lakkis FG, Arakelov A, Konieczny BT, Inoue Y. Immunologic 'ignorance' of vascularized organ transplants in the absence of secondary lymphoid tissue. Nat Med. 2000; 6:686–688. [PubMed: 10835686]
27. Lindquist RL, Shakhar G, Dudziak D, Wardemann H, Eisenreich T, Dustin ML, Nussenzweig MC. Visualizing dendritic cell networks in vivo. Nat Immunol. 2004; 5:1243–1250. [PubMed: 15543150]
28. Loebinger MR, Kyrtatos PG, Turmaine M, Price AN, Pankhurst Q, Lythgoe MF, Janes SM. Magnetic resonance imaging of mesenchymal stem cells homing to pulmonary metastases using biocompatible magnetic nanoparticles. Cancer Res. 2009; 69:8862–8867. [PubMed: 19920196]
29. McCormack DG, Mehta S, Tyml K, Scott JA, Potter R, Rohan M. Pulmonary microvascular changes during sepsis: evaluation using intravital videomicroscopy. Microvasc Res. 2000; 60:131–140. [PubMed: 10964587]
30. McGregor CG, Baldwin JC, Jamieson SW, Billingham ME, Yousem SA, Burke CM, Oyer PE, Stinson EB, Shumway NE. Isolated pulmonary rejection after combined heart–lung transplantation. J Thorac Cardiovasc Surg. 1985; 90:623–626. [PubMed: 3930886]
31. Miller MJ, Wei SH, Parker I, Cahalan MD. Two-photon imaging of lymphocyte motility and antigen response in intact lymph node. Science. 2002; 296:1869–1873. [PubMed: 12016203]
32. Miyao N, Suzuki Y, Takeshita K, Kudo H, Ishii M, Hiraoka R, Nishio K, Tamatani T, Sakamoto S, Suematsu M, Tsumura H, Ishizaka A, Yamaguchi K. Various adhesion molecules impair microvascular leukocyte kinetics in ventilator-induced lung injury. Am J Physiol Lung Cell Mol Physiol. 2006; 290:L1059–L1068. [PubMed: 16387754]
33. Moyron-Quiroz JE, Rangel-Moreno J, Kusser K, Hartson L, Sprague F, Goodrich S, Woodland DL, Lund FE, Randall TD. Role of inducible bronchus associated lymphoid tissue (iBALT) in respiratory immunity. Nat Med. 2004; 10:927–934. [PubMed: 15311275]
34. Murray CJ, Lopez AD. Global mortality, disability, and the contribution of risk factors: global burden of disease study. Lancet. 1997; 349:1436–1442. [PubMed: 9164317]
35. Okazaki M, Gelman AE, Tietjens JR, Ibricevic A, Kornfeld CG, Huang HJ, Richardson SB, Lai J, Garbow JR, Patterson GA, Krupnick AS, Brody SL, Kreisel D. Maintenance of airway epithelium in acutely rejected orthotopic vascularized mouse lung transplants. Am J Respir Cell Mol Biol. 2007; 37:625–630. [PubMed: 17717320]
36. Pena AM, Fabre A, Debarre D, Marchal-Somme J, Crestani B, Martin JL, Beaurepaire E, Schanne-Klein MC. Three-dimensional investigation and scoring of extracellular matrix remodeling during lung fibrosis using multiphoton microscopy. Microsc Res Tech. 2007; 70:162–170. [PubMed: 17177275]
37. Rangel-Moreno J, Moyron-Quiroz J, Kusser K, Hartson L, Nakano H, Randall TD. Role of CXC chemokine ligand 13, CC chemokine ligand (CCL) 19, and CCL21 in the organization and function of nasal-associated lymphoid tissue. J Immunol. 2005; 175:4904–4913. [PubMed: 16210592]
38. Samuel G, Maier LA. Immunology of chronic beryllium disease. Curr Opin Allergy Clin Immunol. 2008; 8:126–134. [PubMed: 18317020]
39. Sommer N, Dietrich A, Schermuly RT, Ghofrani HA, Gudermann T, Schulz R, Seeger W, Grimminger F, Weissmann N. Regulation of hypoxic pulmonary vasoconstriction: basic mechanisms. Eur Respir J. 2008; 32:1639–1651. [PubMed: 19043010]
40. St Croix CM, Leelavanichkul K, Watkins SC. Intravital fluorescence microscopy in pulmonary research. Adv Drug Deliv Rev. 2006; 58:834–840. [PubMed: 16996641]
41. Stefanska AM, Walsh PT. Chronic obstructive pulmonary disease: evidence for an autoimmune component. Cell Mol Immunol. 2009; 6:81–86. [PubMed: 19403056]
42. Tabuchi A, Mertens M, Kuppe H, Pries AR, Kuebler WM. Intravital microscopy of the murine pulmonary microcirculation. J Appl Physiol. 2008; 104:338–346. [PubMed: 18006870]

43. von Garnier C, Filgueira L, Wikstrom M, Smith M, Thomas JA, Strickland DH, Holt PG, Stumbles PA. Anatomical location determines the distribution and function of dendritic cells and other APCs in the respiratory tract. J Immunol. 2005; 175:1609–1618. [PubMed: 16034100]

44. Wagner WW Jr. Pulmonary microcirculatory observations in vivo under physiological conditions. J Appl Physiol. 1969; 26:375– 377. [PubMed: 5773180]

45. Zinselmeyer BH, Dempster J, Wokosin DL, Cannon JJ, Pless R, Parker I, Miller MJ. Chapter 16. Two-photon microscopy and multidimensional analysis of cell dynamics. Methods Enzymol. 2009; 461:349–378. [PubMed: 19480927]

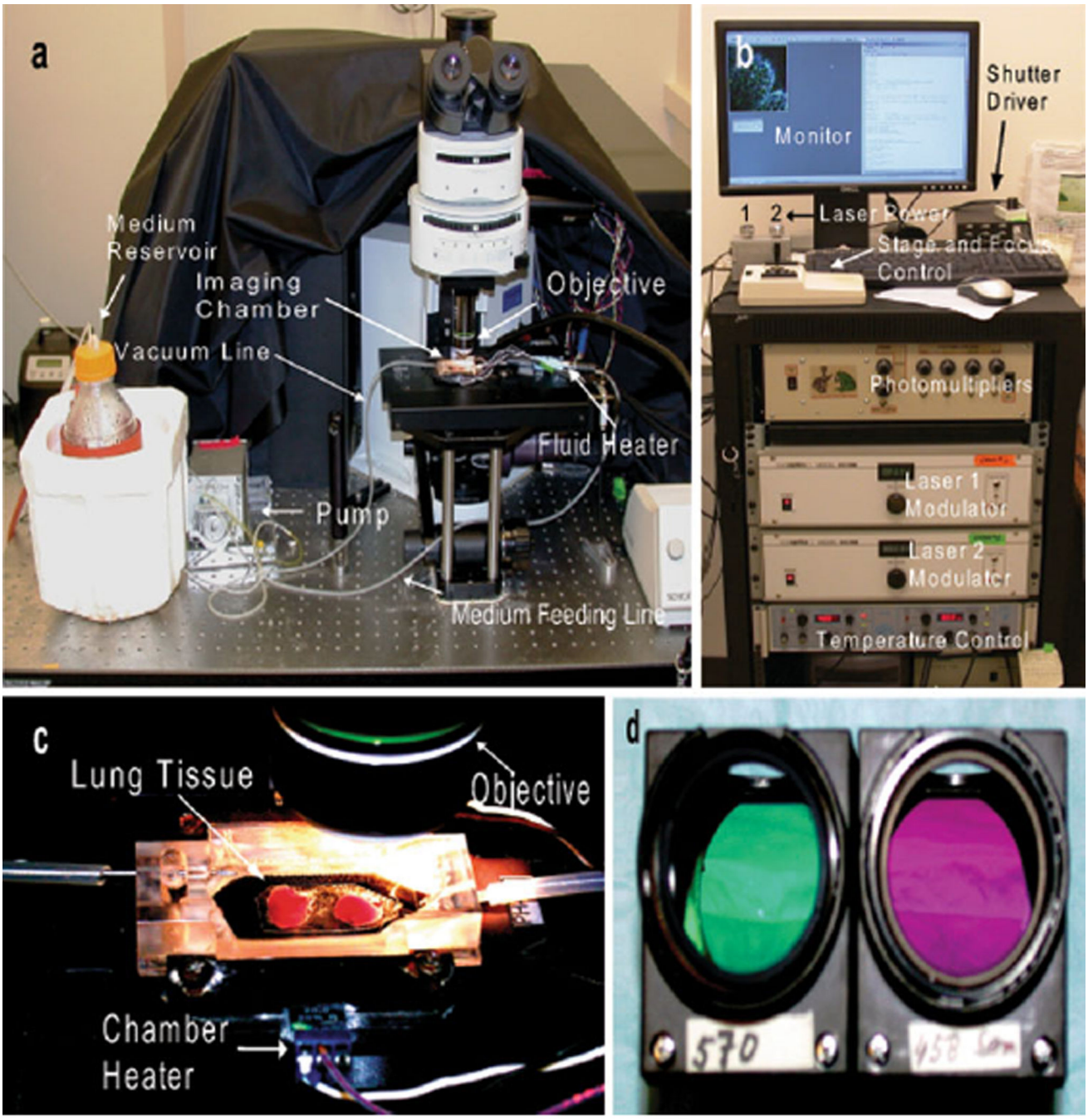

Fig. 1.

Experimental setup for imaging of lung explants with custom-built 2P microscope. **a** Medium is pumped from the reservoir trough a feeding line to the imaging chamber and a vacuum line evacuates the medium from the chamber. The amount of fluid flowing through the chamber is controlled by the pump. The temperatures of the chamber and fluid are maintained at 37°C throughout the experiment with separate heaters. **b** The acquisition console is depicted with multiple components which control the intensity of the laser as well as the movement of the stage and the focus of the objective. Images of the tissue can be

observed on the monitor in real time. **c** Lung tissue is immersed in warm medium within the imaging chamber. **d** Two different filters (570 and 458 nm, respectively) housed inside dichroic cubes. Filters can be exchanged based on experimental design

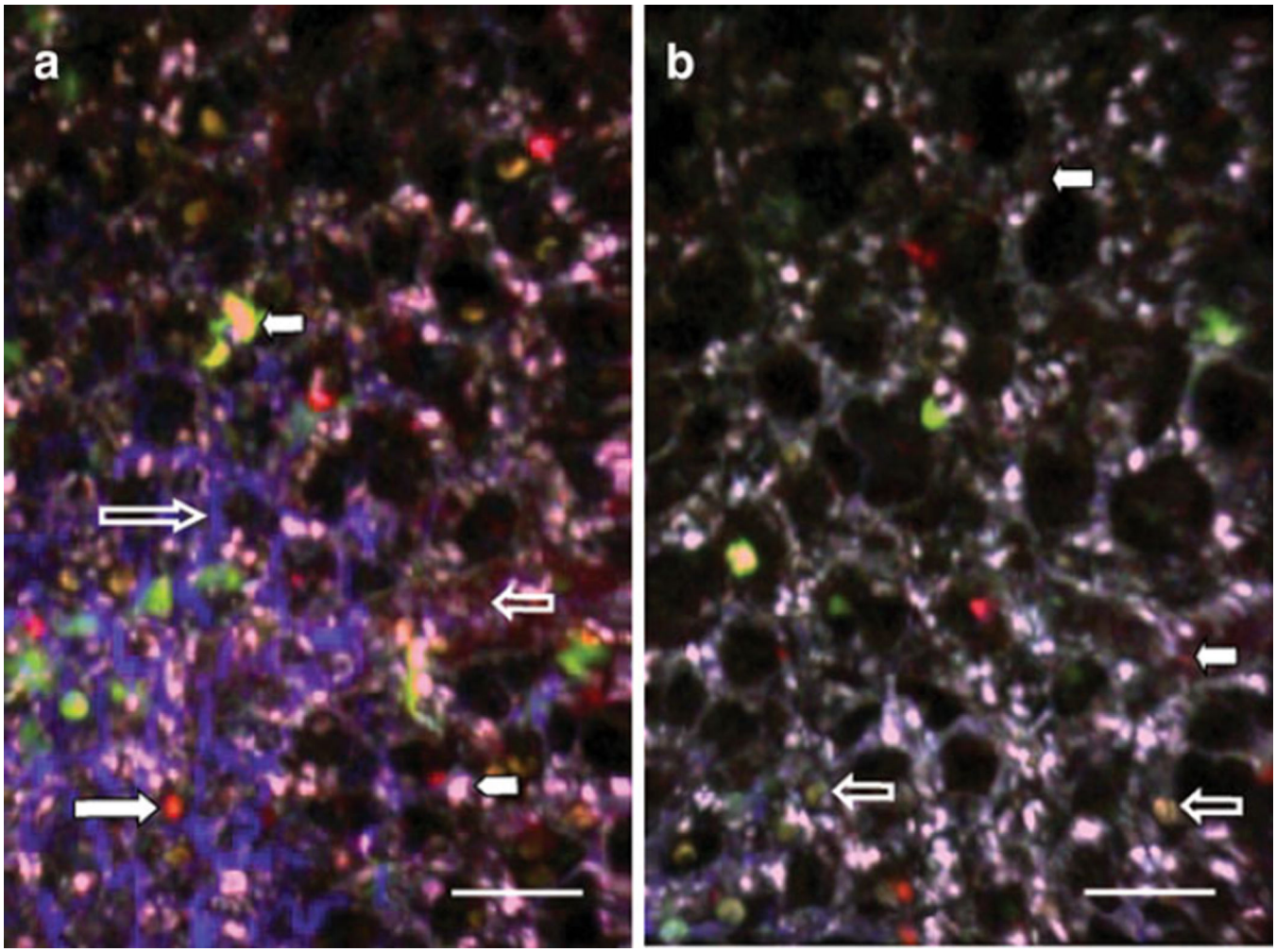

Fig. 2.

2P microscopy of lung explants. Different fluorescent probes were used for this experiment to show the versatility of the system. T cells, isolated from a wild-type C57BL/6 mouse and labeled with fluorescent dyes CMTMR or CMAC, were injected into a C57BL/6 CD11c-EYFP host. The left lung was imaged 24 h after adoptive transfer. **a** Quantum dots (12 μl resuspended in 150 μl of phosphate-buffered saline), injected 10 min prior to sacrifice, label blood vessels in red (*small clear arrow*). T cells labeled with CMTMR are observed in orange (*large white arrow*), and T lymphocytes labeled with CMAC are seen in cyanide (*white arrowhead*). Host CD11c+ cells with dendritic morphology appear yellow-green (*small white arrow*). SHG depicts collagen in blue, which can be seen delineating air spaces (*large clear arrow*). **b** Alveolar macrophages display characteristic nuclear shadow (*clear arrows*). Peri-alveolar blood vessels have been labeled with quantum dots and appear red (*white arrows*). *Space bar* represents 30 μm